ISSN 1547-4771, Physics of Particles and Nuclei Letters, 2020, Vol. 17, No. 2, pp. 142–153. © Pleiades Publishing, Ltd., 2020.

PHYSICS OF ELEMENTARY PARTICLES AND ATOMIC NUCLEI. EXPERIMENT

A New Review of Excitation Functions of Hadron Production in *pp* Collisions in the NICA Energy Range

V. Kolesnikov[a, *], V. Kireyeu[a], V. Lenivenko[a], A. Mudrokh[a], K. Shtejer[a], D. Zinchenko[a], and E. Bratkovskaya[b]

[a] *Joint Institute for Nuclear Research, Dubna, Russia*

[b] *GSI Helmholtzzentrum für Schwerionenforschung GmbH, Darmstadt, Germany; Institut für Theoretische Physik, Johann Wolfgang Goethe-Universitat, Frankfurt am Main, Germany*

**e-mail: Vadim.Kolesnikov@cern.ch*

Received October 17, 2019; revised October 18, 2019; accepted October 18, 2019

Abstract—Data on hadron multiplicities from inelastic proton-proton interactions in the energy range of the NICA collider have been compiled. The compilation includes recent results from the NA61/SHINE and NA49 experiments at the CERN SPS accelerator. New parameterizations for excitation functions of mean multiplicities $\langle\pi^{\pm}\rangle$, $\langle K^{\pm}\rangle$, $\langle K_S^0\rangle$, $\langle\Lambda\rangle$, $\langle p\rangle$, $\langle\overline{p}\rangle$ are obtained in the region of collision energies $3 < \sqrt{s_{NN}} < 31$ GeV. The energy dependence of the particle yields, as well as variation of rapidity and transverse momentum distributions are discussed. A standalone algorithm for hadron phase space generation in *pp* collisions is suggested and compared to model predictions using an example of the PHQMD generator. The investigation has been performed at the Laboratory of High Energy Physics, JINR.

DOI: 10.1134/S1547477120020090

1. INTRODUCTION

The NICA accelerator complex is under construction at JINR (Dubna). It would offer a record luminosity (reaching 10^{27} cm^{-2} c^{-1}) for heavy-ion collisions in the energy range $4 < \sqrt{s_{NN}} < 11$ GeV [1]. Proton-proton collisions at NICA can be studied in the energy range from 4 to 25 GeV. The physics program of the MultiPurpose Detector (MPD) at the NICA collider is aimed at experimental exploration of a yet poorly known region of the QCD phase diagram of the highest net-baryon density with an emphasis on the nature of the transition from hadronic to quark-gluon degrees of freedom, modification of hadron properties in dense nuclear matter, and search for the signals about the critical end point [2]. However, the interpretation of experimental results from nucleus-nucleus interactions showing novel phenomena has to rely on comparison to the corresponding data from elementary collisions. For example, the excitation function of the strangeness-to-entropy ratio, which behaves differently in heavy-ion and *pp* collisions, may serve as an important probe in the study of the deconfinement phase [3] or can be related to chiral symmetry restoration in the dense hadronic matter [4].

Microscopic models of nucleus-nucleus collisions, which utilize multiple physics phenomena in strongly interacting matter, are useful tools for explaining experimental results and making new predictions. Data on hadron yields from elementary inelastic collisions are the essential input for such kind of models permitting to establish details of the evolution of particle inclusive production from elementary to nuclear interactions. Experimental studies of hadron production in *pp* collisions have been performed at many laboratories over 60th–80th of the last century. There are also several review papers, which summarize data and discuss the excitation function of hadron yields in a range of collision energies from several GeV up to LHC energies (see for example [5–7]). These old papers, however, rely on a too broad region of energies as compared to the NICA range and do not include the recent measurements from CERN/SPS [9–14]. Moreover, early bubble chamber applications are typically limited to small data samples (of the order of 10^4 events or so) and have no particle identification, while old spectrometer measurements were done with small solid angle devices and have no sufficient acceptance. In this case extraction of integrated quantities (i.e. mean multiplicities), requiring extrapolation into the unmeasured regions of the reaction phase space, suffers from sizeable systematic uncertainties due the scarcity and incomplete phase space coverage (see for example discussion in [10]). An updated data set of hadron yields, which includes precise measurements from modern detector setups (i.e. NA49 and NA61/SHINE experiments at the CERN/SPS), can allow getting much better parameterizations for the

collision energy dependence of hadron production in the NICA energy range.

Of particular interest is strangeness production. At the lowest NICA energy the excitation function of the production rates of strange hadrons varies strongly due to threshold-dominated effects. Moreover, differences between K^+ and K^- yields related to the underlying production mechanisms are developed at NICA. In this context, since the relation between charged and neutral kaon production is also sensitive to the respective production mechanisms, it is important to examine available data on the K^0 production too.

The aim of this paper is twofold. First, in order to improve the existing elementary data base we want to collect the most complete set of experimental data of hadron yields from *pp* collisions in the NICA energy range, which includes results of mean multiplicities, rapidity distributions, and transverse spectra. Secondly, we want to undertake a systematic study of the collected experimental results as a function of the collision energy and obtain proper parameterizations for the energy dependence of inclusive production cross-sections, as well as investigate the evolution of the parameters of the hadron phase space distributions (i.e. shapes of rapidity spectra and transverse momentum distributions). Since most bulk observables relate to the non-perturbative sector of QCD, it is one of the main goals of this work to obtain the basis for a model independent framework for predicting hadron yields in *pp* collisions at NICA energies. Thus, the results of this study can be used as an input for detector simulation and feasibility study at NICA.

The paper is organized as follows. In Section 2 a new compilation of experimental data on mean hadron multiplicities is presented. The excitation functions for hadron yields are discussed in Section 3. Parameters of the rapidity spectra and transverse momentum distributions for hadron species are discussed in Section 4. In Section 5 we suggest a simulation approach for generation of the hadron phase space distributions based on the obtained parameterizations for the excitation function of particle production yields. A summary in Section 6 closes the paper.

2. EXPERIMENTAL DATA ON HADRON YIELDS FROM *pp* COLLISIONS

In this section we present a collection of experimental data on hadroproduction in inelastic *pp* collisions, which ensures coverage from close to the strangeness production threshold up to the maximum NICA energy.

Early data on charged and neutral hadron production were obtained in 60th–70th years of 20th century by bubble chamber, streamer chamber, and Time-Projection Chamber (TPC) experiments. Later on in a series of experiments at the CERN ISR accelerator (ISR standing for Intersecting Storage Rings) the measurements were performed by counter experiments, where the particle identification was done using Cherenkov and Time-of-Flight (TOF) techniques. Phase space coverage in the most of early experiments required additional extrapolation to get the yield of hadrons in the full momentum space. The details of this procedure are described in the original papers for most of the results presented here (see for example [6]).

Most recently, more accurate and much more detailed data on hadron production in minimum-bias *pp* interactions have been obtained by the NA49 and NA61/SHINE Collaborations at the CERN/SPS accelerator (SPS stands for Super Proton Synchrotron). In the NA49 experiment [15] charged hadrons are identified by energy loss measurement in a large volume TPC tracking system covering a significant fraction of the production phase space. Ionization loss measurements from TPC are complemented by a TOF system, which covers the midrapidity region. Invariant yields of $\pi^\pm$ [9], $K^\pm$ [10], and (anti)protons [11] were measured for the transverse momentum interval from 0 to 2 GeV/c and for the Feynman x variable within $x = [0\ldots0.85]$.

In the framework of the NA61/SHINE experiment [16], the NA49 detector was upgraded with a large solid angle TOF system of 100 ps resolution and faster trigger and read-out electronics. The measurements of charged hadrons in *pp* reactions were performed at five collision energies: $\sqrt{s_{NN}} = 6.2$, 7.6, 8.8, 12.3, and 17.3 GeV. The NA61 Collaboration published rapidity distributions and transverse momentum spectra for charged pions [12, 13], kaons [13], and (anti)protons [13], covering about 1.5 rapidity units in the forward region and the transverse momentum interval from 0 to 2 GeV/c. The hadron yields were then extrapolated to the regions not covered by measurements and the total multiplicities were obtained. Differential spectra, the rapidity distribution and the total yield of Λ-hyperons were obtained only at the top SPS energy [14].

Experimental data on the mean multiplicity of $\pi^\pm$, $K^\pm$, K^0_S, (anti)protons, and Λ are tabulated in Tables 1–4. The compilation includes the results in the energy range slightly wider than the one for NICA: from about 3 GeV (above the threshold energy for strangeness production of ≈2.6 GeV) and up to 31 GeV. In this paper Λ denotes the sum of the average multiplicity of Λ-hyperons produced directly and those originating from electromagnetic decays of Σ^0-hyperons. The statistical and systematic errors of the measurements are added in quadrature, and all the total errors are given in percent relative to the measured value in order to simplify visual recognition of more(less) accurate data.

Table 1. The compiled results on the mean multiplicity of charged pions from inelastic proton-proton interactions at different collision energies

Reference	$\sqrt{s_{NN}}$, GeV	$\langle\pi^-\rangle$	Error, %
[6, 17]	2.99	0.2	10
[6, 17]	3.50	0.29	10
[6, 17]	4.93	0.63	10
[6, 17]	5.03	0.75	10
[17]	5.10	0.72	10
[17]	5.97	0.98	10
[6, 17]	6.12	1.01	10
[12]	6.27	1.05	5
[13]	6.27	1.08	19
[17]	6.38	1.08	10
[6, 17]	6.84	1.11	10
[17]	6.86	1.11	10
[17]	7.43	1.21	10
[12]	7.74	1.31	5
[13]	7.75	1.47	13
[12]	8.76	1.48	3
[13]	8.76	1.71	10
[12]	12.32	1.94	4
[13]	12.32	2.03	9
[6, 17]	13.90	2.19	10
[12]	17.30	2.44	5
[13]	17.30	2.40	8
[10]	17.30	2.36	2
[17]	19.75	2.82	10
[17]	22.02	2.98	10
[10, 17]	30.98	3.44	10
Reference	$\sqrt{s_{NN}}$, GeV	$\langle\pi^+\rangle$	Error, %
[6, 17]	2.99	0.48	10
[6, 17]	3.50	0.67	10
[6, 17]	4.93	1.22	10
[6, 17]	5.03	1.37	10
[6, 17]	6.12	1.6	10
[13]	6.27	1.88	11
[6, 17]	6.84	1.88	10
[13]	7.75	2.08	10
[13]	8.76	2.39	7
[13]	12.32	2.67	5
[13]	17.30	3.11	13
[10]	17.30	3.02	2
[17]	22.02	3.56	10
[10, 17]	30.98	4.04	10

Table 2. The compiled results on the mean multiplicity of charged kaons from inelastic proton-proton interactions at different collision energies

Reference	$\sqrt{s_{NN}}$, GeV	$\langle K^-\rangle$	Error, %
[6, 17]	5.03	0.0095	35
[6, 17]	6.15	0.036	14
[13]	6.27	0.024	26
[6, 17]	6.84	0.031	14
[13]	7.75	0.045	11
[6]	7.86	0.05	30
[6, 17]	8.21	0.07	29
[13]	8.76	0.084	8
[6, 17]	9.08	0.08	25
[6, 17]	9.97	0.11	27
[6, 17]	11.54	0.13	23
[13]	12.32	0.095	7
[13]	17.30	0.132	11
[10]	17.30	0.13	10
[17]	22.02	0.24	10
[10]	23.00	0.171	15
[6]	23.68	0.209	15
[6]	30.59	0.244	15
[10, 17]	30.98	0.245	10
Reference	$\sqrt{s_{NN}}$, GeV	$\langle K^+\rangle$	Error, %
[6]	2.98	0.0046	15
[6, 17]	2.99	0.0035	16
[6]	2.99	0.0044	18
[6]	3.12	0.0057	18
[6]	3.35	0.0069	15
[6, 17]	3.50	0.008	21
[6]	4.11	0.02	20
[6, 17]	5.03	0.07	43
[6]	5.35	0.054	10
[6, 17]	6.15	0.107	2
[13]	6.27	0.097	14
[6, 17]	6.84	0.1188	1 3
[13]	7.75	0.157	12
[13]	8.76	0.17	15
[6, 17]	11.54	0.21	28
[13]	12.32	0.201	7
[13]	17.30	0.234	9
[10]	17.30	0.227	5
[17]	22.02	0.35	10
[10]	23.00	0.273	15
[6]	23.68	0.337	15
[6]	30.59	0.367	15
[10, 17]	30.98	0.3562	13

Table 3. The compiled results on the mean multiplicity of $\langle K_S^0 \rangle$ and $\langle \Lambda \rangle$ from inelastic proton-proton interactions at different collision energies

Reference	$\sqrt{s_{NN}}$, GeV	$\langle K_S^0 \rangle$	Error, %
[6]	2.98	0.00083	22
[6]	3.35	0.0019	16
[6, 17]	3.50	0.00364	3
[6]	3.63	0.0034	9
[6]	3.85	0.0064	8
[6]	4.08	0.0072	8
[6, 17]	4.93	0.0202	2
[6, 17]	5.01	0.023	2
[6, 17]	6.12	0.0415	3
[6, 17]	6.84	0.0495	2
[6]	6.91	0.045	9
[6]	11.45	0.109	6
[6]	13.76	0.122	8
[6, 17]	13.90	0.141	10
[6]	16.66	0.158	4
[6]	19.42	0.16	13
[6]	19.66	0.181	8
[10]	23.00	0.222	10
[6]	23.76	0.224	8
[6]	26.02	0.26	4
[6]	27.43	0.2	10
[6]	27.60	0.232	5
[10, 17]	30.98	0.274	10
Reference	$\sqrt{s_{NN}}$, GeV	$\langle \Lambda \rangle$	Error, %
[6]	2.98	0.0033	18
[18]	3.17	0.0073	4
[6]	3.35	0.0073	4
[6, 17]	3.50	0.0127	9
[6]	3.63	0.0109	6
[6]	3.85	0.0172	6
[6]	4.08	0.0201	5
[6, 17]	4.93	0.0388	2
[6, 17]	5.01	0.035	11
[6, 17]	6.12	0.061	3
[6, 17]	6.84	0.0657	1
[6]	6.91	0.037	19
[6]	11.45	0.109	6
[6]	13.76	0.112	12
[6, 17]	13.90	0.099	12
[6]	16.66	0.133	5
[13]	17.30	0.12	9
[6]	19.42	0.08	25
[6]	19.66	0.103	11
[6]	23.76	0.111	14
[6]	23.76	0.11	9
[6]	26.02	0.12	17
[6]	27.43	0.12	8
[6]	27.60	0.125	6

Table 4. The compiled results on the mean multiplicity of $\langle p \rangle$ and $\langle \bar{p} \rangle$ from inelastic proton-proton interactions at different collision energies

Reference	$\sqrt{s_{NN}}$, GeV	$\langle p \rangle$	Error, %
[6, 17]	3.50	1.56	10
[6, 17]	4.93	1.68	10
[6, 17]	5.01	1.55	10
[6, 17]	6.12	1.41	10
[6, 17]	6.15	1.69	10
[13]	6.27	1.154	4
[6, 17]	6.84	1.615	10
[13]	7.75	1.093	6
[13]	8.76	1.095	8
[13]	12.32	0.977	14
[13]	17.30	1.069	12
[10]	17.30	1.162	15
[17]	22.02	1.28	10
[10, 17]	30.98	1.34	10
Reference	$\sqrt{s_{NN}}$, GeV	$\langle \bar{p} \rangle$	Error, %
[6, 17]	6.15	0.0023	10
[13]	6.27	0.0047	15
[6, 17]	6.84	0.004	10
[13]	7.75	0.0047	16
[6, 17]	8.21	0.005	10
[13]	8.76	0.0059	12
[6, 17]	9.08	0.008	10
[6, 17]	9.97	0.011	10
[6, 17]	11.54	0.015	10
[13]	12.32	0.0183	10
[13]	17.30	0.0402	9
[10]	17.30	0.039	15
[17]	22.02	0.061	10
[10, 17]	30.98	0.11	10

In addition to that, in Table 5 are tabulated the results for π^- obtained from the measurements of negatively charged hadrons (h^-) from [8]. The contribution from K^- and antiprotons in the h^- yields was subtracted by us, the correction procedure is described in Section 3.3.

Special emphasis should be put here on the problem of the contribution from weak decays of strange particles in the measured multiplicities of pions and (anti)protons. The size of this contribution depends on the collision energy and used experimental technique. In bubble chamber experiments of a small detector size most weak decays escape the fiducial vol-

Table 5. The results on mean multiplicities $\langle\pi^-\rangle$ calculated from the data for negatively charged hadrons $\langle h^-\rangle$ [8] in inelastic proton-proton interactions at different collision energies. The calculation procedure is described in the text

Reference	$\sqrt{S_{NN}}$, GeV	$\langle\pi^-\rangle$ ($\langle h^-\rangle$)	Error, %
[8]	2.98	0.170	14
[8]	3.5	0.352	3
[8]	3.78	0.429	5
[8]	4.93	0.707	2
[8]	6.12	0.985	2
[8]	6.84	1.08	2
[8]	8.29	1.33	2
[8]	9.78	1.60	4
[8]	10.69	1.705	4
[8]	11.46	1.82	3
[8]	13.76	2.07	2
[8]	13.9	2.02	3
[8]	16.66	2.34	3
[8]	18.17	2.57	5
[8]	19.42	2.65	3
[8]	19.66	2.63	3
[8]	21.7	2.72	4
[8]	23.88	3.09	3
[8]	26.02	3.26	3

ume and the remaining secondary decay vertices can be easily reconstructed, thus the daughters are eliminated from the analysis. In contrast, for fixed target experiments with long detectors a sizeable fraction of the weak decay products populate the data sample due to limited vertex finding performance in such setups. In the data collection, presented here, there is no unique approach to deal with the feeddown correction: in [9, 11] the contribution from weak decays was subtracted, in [13] it was partially eliminated by track selection criteria, while in many fixed target experiments from the last century decay products partially counted into the total sample without any attempt to make a correction for their contribution. As a reference estimate of the size of such a correction we can refer to [9], where a complete feed-down subtraction procedure for charged pions from *pp* reactions at $\sqrt{s_{NN}} = 17.3$ GeV was performed by considering all relevant sources (i.e. K^0_S, Λ, Σ^0, $\Sigma^\pm$). The authors found that the feed-down pions are mostly concentrated at low p_t near midrapidity having percentage of 6% for π^+ and 10% for π^-. Of course, the overall (integrated over the full phase space) feed-down contribution is smaller, nevertheless, an additional systematic uncertainty to the results on pion multiplicities reported by early experiments (of the order of 3–5%) should be kept in mind.

3. STUDY OF THE EXCITATION FUNCTION OF THE MEAN MULTIPLICITY OF HADRONS

In the following subsections we discuss the excitation functions of hadron yields specie by specie.

3.1. Kaons

We begin with kaons because these results are used in Section 3 to obtain the yields of π^- from those of negatively charged hadrons. The energy dependence of the mean multiplicity of charged kaons $\langle K^\pm\rangle$ from minimum-bias *pp* collisions is shown in Fig. 1a. A strong dependence of the kaon production rates on $\sqrt{s_{NN}}$ is observed at low NICA energies due to threshold-dominated effects. In order to describe the excitation function of the hadron production rates we used two parameterizations. The first one (*Fit1*) represents a fit to the form

$$\langle n\rangle = a + \frac{b}{\sqrt{s}} + c\ln s, \quad (1)$$

with 3 parameters (a, b, c), which was suggested in [19] based on a general analysis of hadron multiplicities including Redge trajectory with intercept one-half.

In addition, we used a parameterization based on the Lund–String–Model (LSM) from [20] (*Fit2*) given by

$$\langle n\rangle = a(x-1)^b (x)^{-c}, \quad (2)$$

where $x = s/s_0$, s is the square of the center-of-mass energy, s_0 is the square of the production threshold, and (a, b, c) are the fit parameters.

The fit results are plotted in Fig. 1a with a dashed and solid line for *Fit1* and *Fit2*, respectively. We found that both parameterizations describe the energy dependence of hadron multiplicities through the NICA energy range equally good, while *Fit2* is slightly better describes the overall trend (see Fig. 1b and Fig. 3).

As it was underlined in the Introduction, it is interesting to look at the available data on K^0_S production, because the relation between charged and neutral kaons is also strongly related to the competitive strangeness production mechanisms. The energy dependence for the mean multiplicity of K^0_S from *pp* collisions is shown in Fig. 1b. Fits to Eqs. (1) and (2) are shown by dashed and solid lines, respectively. Because of isospin conservation in strong interactions, the production of charged and neutral kaons species is

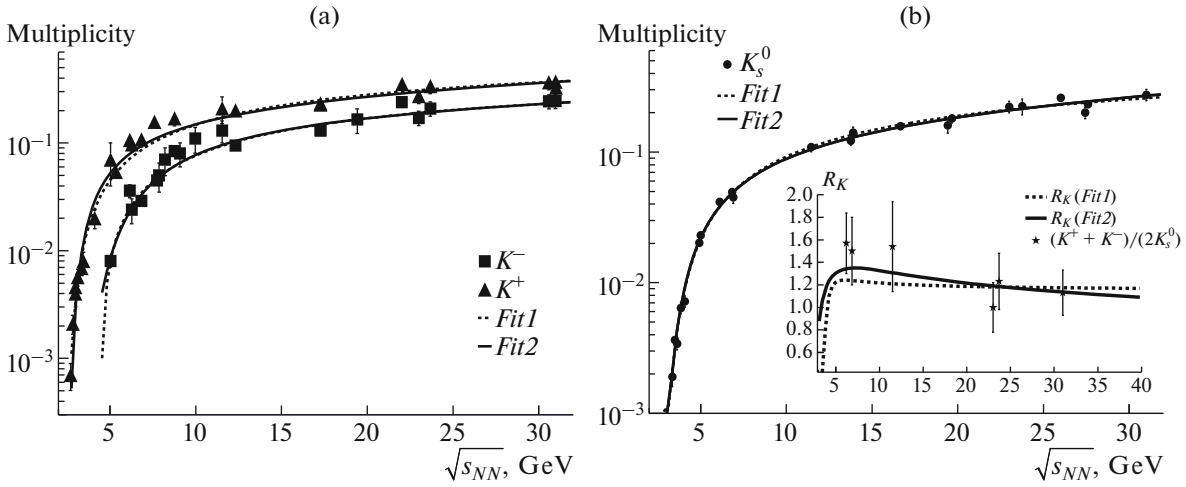

Fig. 1. (a) The energy dependence of the multiplicity of charged kaons in inelastic pp collisions (data from Table 2). Fits to Eqs. (1) and (2) are shown by dashed and solid lines, respectively (see text for details). (b) The multiplicity of K_S^0 as a function of $\sqrt{s_{NN}}$ in inelastic pp collisions (data from Table 3). Fits to Eqs. (1) and (2) are shown by dashed and solid lines, respectively. In the inset the R_K-ratio is plotted as a function of center-of-mass energy for the two discussed parameterizations (dashed and solid lines) and for kaon measurements (symbols).

equally probable, thus, from isospin invariance one expects the ratio

$$R_K = \frac{0.5\left(\left\langle n_{K^+}\right\rangle + \left\langle n_{K^-}\right\rangle\right)}{\left\langle n_{K_S^0}\right\rangle}$$

to be equal to unity (only half of the produced neutral kaons is considered as K_L^0 is difficult to register due to its long lifetime).

The inset in Fig. 1b indicates the energy dependence for R_K taken as the ratio of the parametrized excitation functions of kaon multiplicities for *Fit1* (dashed line) and *Fit2* (solid line). Moreover, among all the collected data points we found those where all kaon sorts (i.e. K^+, K^-, K_S^0) are measured at the same energy or at very closed energies. Thus, the R_K ratio was calculated from this subset of measurements and shown in the inset of Fig. 1b by stars. As can be seen, R_K approaches unity with increasing energy, still, deviating from the isospin invariance motivated kaon production ratio in the NICA energy range. We also found that the results for *Fit2* slightly better describe the trend for R_K. Since the experimental errors in the discussed kaon measurements are large, we can not argue that the observed deviation in the R_K-ratio from the expected value might be an indicator of some anomaly in the kaon production in pp interactions at NICA energies (as non-trivial interference of multiple isospin production channels or a signal for isospin fluctuations in kaon sector). New high precision measurements for all kaon species in the NICA energy range can potentially unveil this mystery.

One advantage concerning the kaon data is the absence of feed-down from weak decays, except the contribution from decays of Ω-hyperons, which is negligibly small at NICA energies. From other side, the contribution from decays of resonances (as ϕ(1020)) needs to be (at least) estimated. Avoiding the region of collision energies close to the production threshold, the ratio $\langle\phi\rangle/\langle\pi\rangle \approx 0.004$ can be obtained from a number of measurements in the NICA energy range [21]. Taking into account the averaged charged pion yield and the branching to charged and neutral kaons we estimate at the top NICA energy the ϕ-meson contribution to the production rates of kaons as: 2.1% for K^+, 3.6% for K^-, and <1% for K_S^0. These numbers are well below the errors quoted in the data compilation, so we neglect this contribution.

3.2. (Anti)protons and Λ-Hyperons

Experimental data for the mean multiplicity of protons and antiprotons from pp interactions in the NICA energy range are scarce. In the case of antiprotons the reason is the low production cross section, thus very large data sets have to be collected to provide sufficient statistics. However, the experimental technique in old (mostly bubble chamber) experiments did not allow to collect large volume data sets, only very recently such measurements became available from SPS [11, 13]. For the case of protons the reason of small number of inclusive measurements is different. Since protons in pp reactions at NICA are mainly produced from fragmentation of strings (with small addition from decays of Δ resonances), their distributions in rapidity have a non-trivial shape (see Fig. 5b). Since

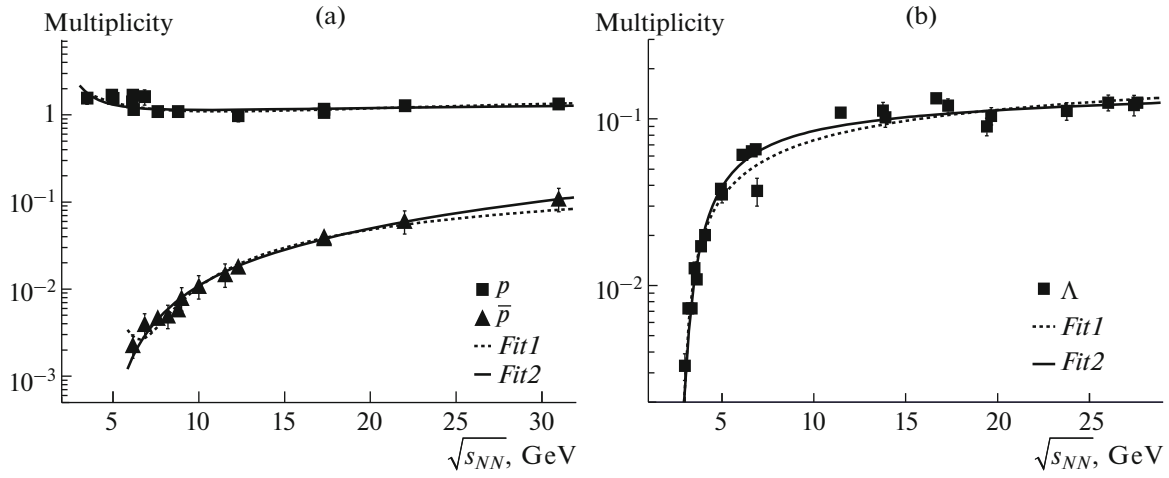

Fig. 2. (a) The energy dependence of the multiplicity of charged protons and antiprotons in inelastic *pp* collisions (data from Table 3). Fits to Eqs. (1) and (2) are shown by dashed and solid lines, respectively. (b) The energy dependence of the multiplicity of Λ in inelastic *pp* collisions (data are from Table 4).

measurements over a limited acceptance does allow to do easy extrapolation to unmeasured regions, only experiments with a wide phase space coverage can provide valuable data for protons (actually, a close to 2π-coverage in the forward/backward direction is sufficient).

The energy dependence for the mean multiplicity of protons and antiprotons is shown in Fig. 2a. There is a small variation of the proton's multiplicity in the NICA energy range, which is expected for a leading particle. The local minimum of the yield of protons is reached at about 10 GeV and further increase can be roughly accounted by the gain in the number of the produced baryon-antibaryon pairs. In contrast, the production of antiprotons grows rapidly at low NICA energies, exhibiting a kind of threshold behavior up to large $\sqrt{s}$ values.

Measurements of Λ-hyperon production in the energy range of NICA are mainly performed by bubble chamber experiments and only a single data point was obtained recently by the SPS NA61/SHINE experiment at $\sqrt{s_{NN}} = 17.3$ GeV [14]. The results for Λ-hyperons are presented in Fig. 2b. After a rapid increase close to the threshold, the Λ production rate is close to saturation at NICA energies.

3.3. Charged Pions

Now we come to the most abundant species—charged pions. In Fig. 3a the mean multiplicity of charged pions in *pp* interactions is plotted as a function of the collision energy. The experimental data for π^- and π^+ are drawn by squares and triangles, respectively. In order to get the yield of π^- from the measurements of negatively charged hadrons from [8] the following procedure was used. For each data point (for each $\sqrt{s_{NN}}$ value) the mean multiplicities of K^- and antiprotons from the known parameterizations for their energy dependences (see Sections 3.1 and 3.2) were subtracted. For this we used the results for the parameterization with *Fit2*. The uncertainty of this correction (calculated by propagating the fit errors) was added in quadrature to the measurement error. The resulting negatively charged pion multiplicities are drawn in Fig. 3a by stars. The drawn in figure lines are the parameterizations according to Eqs. (1) and (2).

The overall quality of the obtained parameterizations for hadrons can be tested if the excitation function of the charge balance will be obtained. Conservation of charge in *pp* reactions requires that the difference between positive and negative particle multiplicities should give two units. In Fig. 3b the difference between the sum of the multiplicities for all positively charged hadrons $\Sigma^+ = \langle n_{\pi^+} \rangle + \langle n_{K^+} \rangle + \langle n_p \rangle$ and negatively charged hadrons $\Sigma^- = \langle n_{\pi^-} \rangle + \langle n_{K^-} \rangle + \langle n_{\bar{p}} \rangle$ is plotted. All the numbers are obtained from the two used parameterizations of data points drawn in Figs. 1–3. The difference $\Sigma^+ - \Sigma^-$ is also accounts for the charge balance of charged hyperons $\langle n_{\Sigma^+} \rangle - \langle n_{\Sigma^-} \rangle \approx 0.23 \langle n_{\Lambda+\Sigma^0} \rangle$, the coefficient 0.23 was obtained from models. We found that the overall charge balance is off from the nominal value (=2) not larger than by 0.13 units, so all the multiplicities computed from the obtained parameterizations are consistent with charge conservation within 5.9 and 1.5% for *Fit1* and *Fit2*, respectively.

Finally, the inclusive production cross-sections for $\pi^\pm$, $K^\pm$, K^0_S, Λ, and (anti)protons are drawn in Fig. 4. They are calculated as $\sigma = \langle n \rangle \sigma_{\text{in}}$, where $\langle n \rangle$ is the

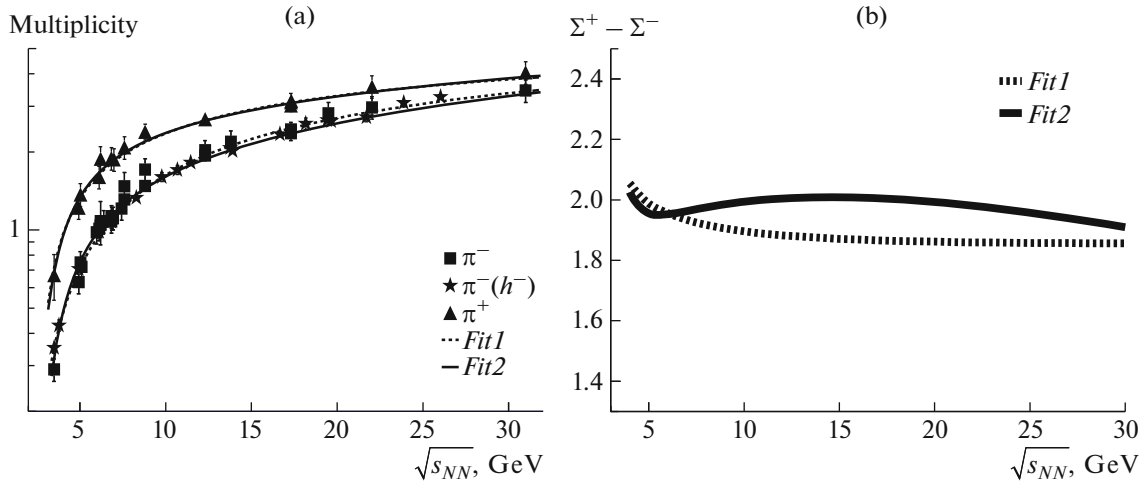

Fig. 3. (a) The energy dependence of the multiplicity of charged pions in inelastic *pp* collisions (data from Tables 1, 5). Fits to Eqs. (1) and (2) are shown by dashed and solid lines, respectively. b)The sum of the multiplicities of positively charged hadrons Σ^+ minus Σ^- for all negatively charged ones (taken from the parameterizations for the hadron excitation functions) as a function of $\sqrt{s_{NN}}$ (see text for details).

hadron multiplicity and σ_{in} is the inelastic cross-section. The latter was calculated according the parameterization from [22]. We used the functional form according to Eq. (2) to parametrize the energy dependence for the cross-sections and the fit parameters of the plotted lines for all hadrons are tabulated in Table 6. As one can see, χ^2/NDF lies in the range from 0.5 to 2.4 for all hadrons, except Λ. In the latter case, the goodness of the fit can be evaluated visually (see Fig. 2b), while a greater value of χ^2 can be explained by larger scattering of data points around the best fit line and by a couple of outliers (i.e. measurements deviating more than 3σ from the prediction).

4. RAPIDITY AND TRANSVERSE MOMENTUM DISTRIBUTIONS FOR HADRONS FROM *pp* REACTIONS

In this section we discuss rapidity and transverse momentum distributions of hadrons from *pp* collisions. In Fig. 5a rapidity distributions for negatively charged kaons and pions are shown. These data from the NA61 experiment [12, 13] were taken at five collision energies ($\sqrt{s_{NN}}$ from 6 to 17 GeV). The data points were normalized by us to the mean multiplicity $\langle n \rangle$ and plotted as a function of the scaled rapidity y/y_{beam}, where y_{beam} is the rapidity value for the projectile proton. Since the discussed measurements are only performed in the forward hemisphere ($y/y_{\mathrm{beam}} > 0$), we have added the points in the backward hemisphere due to reflection symmetry with respect to the midrapidty in *pp* reactions. As can be seen, the rapidity dependence of the yields of pions and kaons follows a bell-like shape at all energies. Moreover, the normalized distributions have little shape variation within the energy interval $6 < \sqrt{s_{NN}} < 17$ GeV. Thus, Gaussian fits were applied to the collection of rapidity spectra at all energies keeping the position of the maximum fixed at midrapidity. The resulting fit functions are plotted by dashed lines. The same procedure was applied to positively charged pions and kaons (not shown here) and the parameter σ of the Gaussian function give us

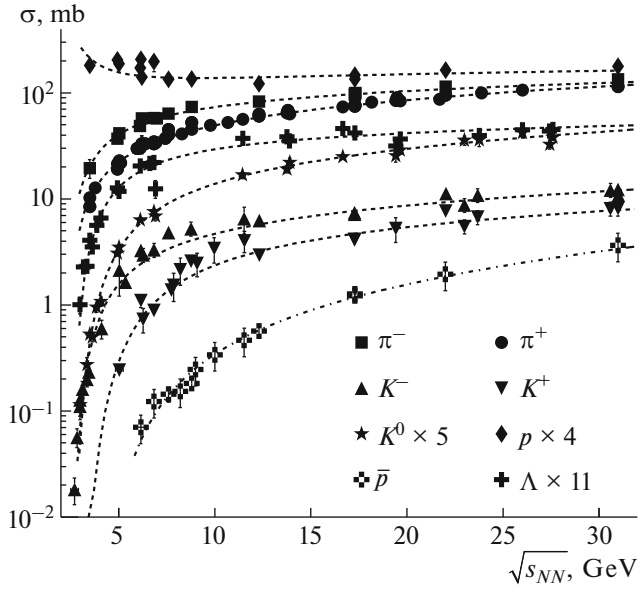

Fig. 4. Inclusive hadron production cross-sections from *pp* interactions as a function of the center-of-mass energy. Dashed lines are parameterizations to Eq. (2).

Table 6. Parameterization parameters (according to Eq. (2)) for the hadron production cross-sections

Hadron	a	b	c	s_0 (GeV^2)	χ^2/NDF
π^-	18.79 ± 0.554	1.998 ± 0.089	–.653 ± 0.095	4.64	0.5
π^+	43.046 ± 13.69	2.366 ± 1.386	2.168 ± 1.454	4.07	0.5
K^-	1.509 ± 0.363	5.138 ± 0.801	4.783 ± 0.853	8.2	2.0
K^+	2.176 ± 0.26	2.63 ± 0.155	2.285 ± 0.181	6.49	2.4
K_S^0	1.151 ± 0.087	3.697 ± 0.122	3.284 ± 0.139	6.49	1.9
p	19.49 ± 1.824	–8.717 ± 0.054	–8.823 ± 0.054	0	1.3
$\bar{p}$	0.122 ± 0.004	3.511 ± 0.291	2.69 ± 0.271	14.08	0.8
Λ	2.066 ± 0.161	2.625 ± 0.102	2.468 ± 0.121	6.49	4.1

the value of 0.37, 0.49, 0.51, and 0.55 for K^-, π^-, K^+, and π^+, respectively.

In Fig. 5b scaled by the mean multiplicity rapidity distributions for protons from minimum bias pp reactions at five collision energies are shown. The data points are taken from [13] and the measurements at forward rapidities are reflected to the backward hemisphere assuming symmetry of the distribution around midrapidity. As one can see, rapidity spectra of protons in contrast to mesons and antiprotons have a broad minimum at midrapidity rising rapidly towards beam (target) rapidity. Moreover, the dip of the minimum increases with collision energy indicating increase of the rapidity loss by initial protons in the course of the reaction, leading to the increase of the rapidity density of particles (mostly mesons) produced near midrapidity. We found that the shape of rapidity spectra for protons can be parametrized by a symmetric polynomial of 6th order $dN/dy \approx a(y/y_{\text{beam}})^6 + b(y/y_{\text{beam}})^2 + c$, where the coefficients of the parabolic part of the fit function (b and c) describe the behavior near midrapidity and normalization, while a negative coefficient a defines sharp drop of the rapidity spectra at the beam rapidity. An example of a fit with a symmetric polynomial of 6th order to the data at 7.6 GeV is drawn in Fig. 5b as a dashed line. The same parameterization can describe the rapidity spectrum of Λ-hyperons (not shown).

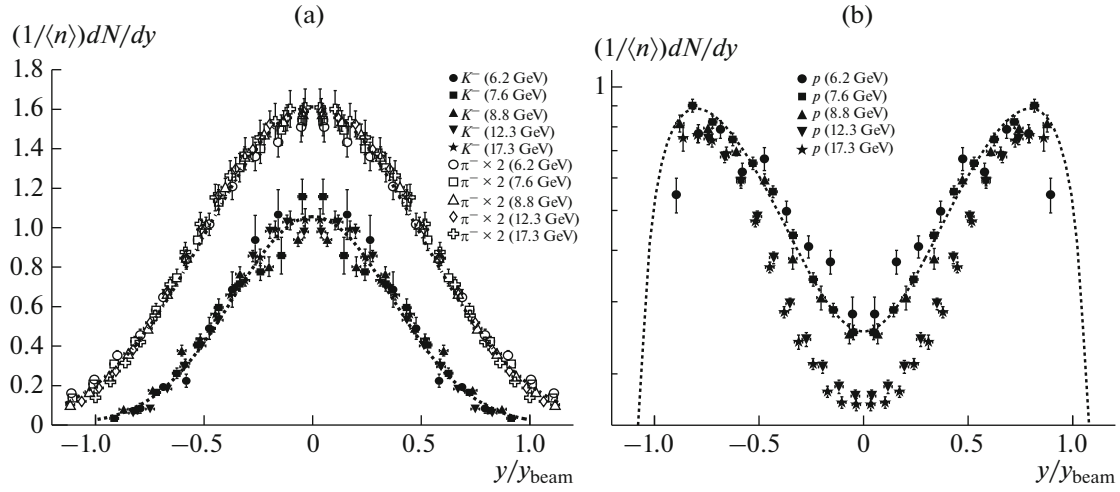

Fig. 5. (a) The scaled yield of K^- and π^- as a function of normalized rapidity y/y_{beam} in inelastic pp collisions at 6.2–17.3 GeV. The experimental data are taken from [13] and [12] and center-of-mass collision energy is given in the parenthesis. The numbers for π^- are multiplied by 2 for clarity, the dashed lines indicate fits to Gaussian function (see text for details). (b) The scaled yield of protons as a function of normalized rapidity y/y_{beam} in inelastic pp collisions at 6.2–17.3 GeV. The experimental data are taken from [13] and center-of-mass collision energy is given in the parenthesis. The dashed line indicate a fit to the data at 7.6 GeV with a symmetric function of 6th order (see text for details).

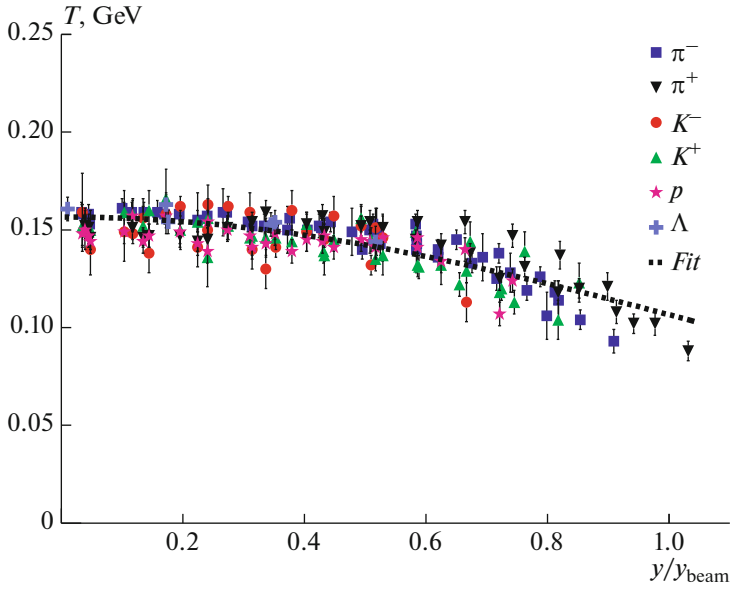

Fig. 6. The slope parameter T for hadrons in bins of normalized rapidity y/y_{beam} from inelastic pp collisions at 6.2–17.3 GeV. The experimental data are taken from [12–14]. The dashed line indicate a fit to a Gaussian function (see text for details).

Transverse momentum distributions of hadrons from high-energy particle collisions are usually described by a Bose–Einstein distribution with the inverse slope parameter T (effective temperature). A collection of slope parameters values for hadrons from pp collisions are plotted in Fig. 6 as a function of normalized rapidity y/y_{beam}. The experimental data are taken from [12–14], and for each hadron specie we combined the measurements at all collision energies together. The rapidity dependence for the slope parameter follows a Gaussian shape at all energies and for all hadrons. It is interesting to note that for each hadron we found little variation of the shape of the rapidity distributions for the slope parameter with collision energy in the energy range from 6 to 17 GeV. Moreover, the shapes are similar for all hadrons. The latter was checked by comparing the results of fitting of the rapidity distribution for each hadron to a Gaussian: we found that the results for the fit parameters vary by less than 3% for the amplitude (the slope at the mean rapidity) and by 2% for the standard deviation. A Gaussian shape with the averaged over all hadron specie parameters ($T(0) = 157$ MeV, $\sigma = 1.1$) is plotted in Fig. 6 by a dashed line, and, indeed, as one can see, the measurements are tightly concentrated around this line.

Antiprotons (not shown), however, do not follow the common trend. The slope parameter for $\bar{p}$ appears to be rising (by about 40%) in the NICA energy range, still lying below the common trend for other hadrons (from 20 to 60% down depending on collision energy).

5. PHASE SPACE DISTRIBUTIONS OF HADRONS FROM pp REACTIONS: DATA VERSUS MODEL

A number of feasibility studies to ensure optimal detector performance under different experimental conditions at the NICA collider requires efficient and realistic hadron phase space Monte Carlo generation. For this, dedicated software libraries—event generators, may be used to predict high-energy particle physics events. A list of microscopic models on the market includes UrQMD [23], EPOS [24], PHSD [25], and PHQMD [26] generators. Despite of the fact that some models reproduce moderately well the energy dependence of hadron yields, none of the existing event generators can simultaneously describe total multiplicities, rapidity spectra, and transverse momentum distributions. In order to overcome this challenge we suggest a simple particle generator to obtain realistic hadron phase space distributions using the results of the analysis of hadron production, which were discussed in previous Sections. The generator provides $\langle n \rangle$ particles of a particular sort per event followed a predefined profile along rapidity (Gaussian for produced mesons or polynomial for p, Λ) and thermally distributed along transverse momentum. The parameters $\langle n \rangle$, σ_{Gauss}, and T (slope) are taken from parameterizations discussed in Sections 3, 4. Owning to the fact that we are only interested in the phase space regions covered by the experimental setup at the NICA collider, a short description of the detector and its simulation process will be given.

The MPD (Multi-Purpose Detector) detector at NICA comprises large coverage of the reaction phase

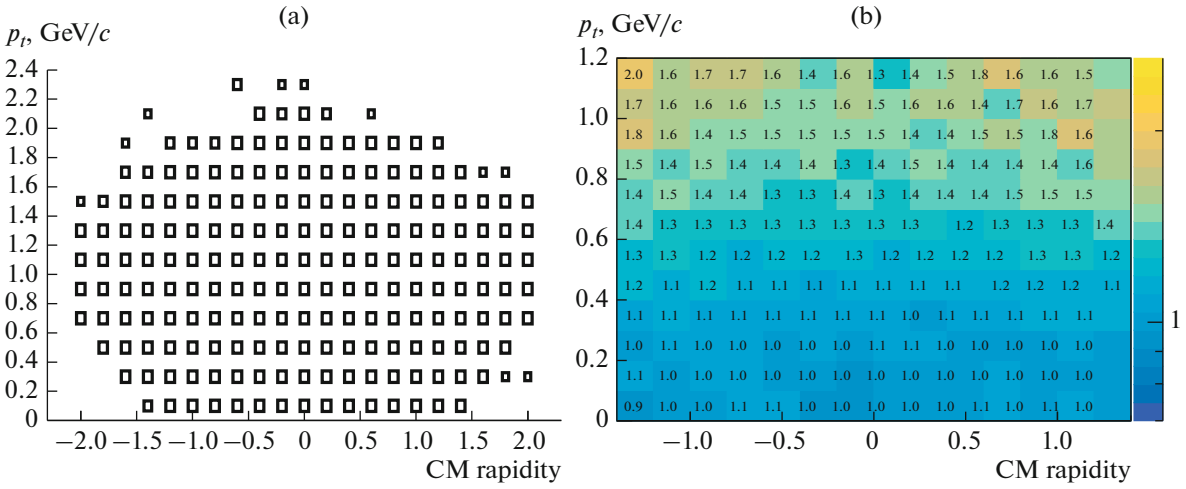

Fig. 7. Left: Phase space coverage of the MPD detector for positively charged kaons in pp collisions at $\sqrt{s} = 9$ GeV in terms of center-of-mass rapidity and transverse momentum. The parameterization of the kaon phase space used as the simulation input is based on experimental data (see text for details). (Color online) Right: The ratio of K^+ production rates $d^2N/(dp_t dy)$ from the PHQMD model [26] and from the particle generator (pp collisions at $\sqrt{s} = 9$ GeV).

space together with precise tracking and particle identification capabilities [2]. Simulation of high-energy particle interactions is performed within a dedicated software framework—MPDRoot [27] which consists of a geometry toolkit for detector description, track propagation routines based on the GEANT package, and multiple algorithms for detector response simulation and event reconstruction. A set of dedicated interfaces, written in the implementation language of ROOT (C++), allows easy transformation of the particle parameters from multiple event generators to the input of the GEANT package to be propagated through the detector. All the tracks which are registered in the detector elements are kept for further analysis. The results of the simulation procedure for positively charged kaons with the suggested particle phase space generator are shown in Fig. 7 (left panel), where the phase space coverage of kaons registered in the MPD setup is plotted in terms of center-of-mass rapidity and transverse momentum. As one can see, the coverage in both longitudinal and transverse momentum components is sufficiently large, so reliable representation of hadron phase space used as an input for simulation is, indeed, crucial. The latter can be illustrated by comparing the predictions of the suggested particle generator and different models. Testing all mentioned above event generators we found that the minimal difference between hadron production rates (particle generator versus model) over the entire MPD detector acceptance is in the case of the PHQMD model.

The novel microscopic n-body dynamical transport approach PHQMD (Parton-Hadron-Quantum-Molecular-Dynamics) is based on quark, diquark, string, and hadronic degrees of freedom and extends the collision integral from the established PHSD (Parton-Hadron-String-Dynamics) approach [25, 28] uniting it with 2-body potential interactions between baryons. While high energy inelastic hadron-hadron collisions in PHQMD are described by the FRITIOF string model [29], the transport approach at low energy hadron–hadron collisions is based on experimental cross sections and matched to reproduce the nucleon–nucleon, meson–nucleon and meson–meson cross section data in a wide kinematic range. In the string fragmentation process, implemented in the model, strangeness production is governed by addition parameters, which define the probability to create a strange quark–antiquark pair or diquark–antidiquark pair. In Fig. 7 (right panel) is shown the ratio of K^+ production rates ($d^2N/(dp_t dy)$) from the PHQMD model and from our particle phase space generator. As one can see, the model reasonable well describes the kaon production near midrapidity and at low transverse momenta. At larger momenta, however, the difference in the production rates between experimental data and model is growing progressively, thus, overall transverse dynamics in the PHQMD generator needs some additional tuning to reproduce data.

Finally, we can point out that the suggested simple particle phase space generator, which describes hadron production phase space in pp collisions based on experimental data, can be very useful for testing available event generators and performing detector performance studies in the NICA energy range.

6. SUMMARY

Using existing experimental data for elementary *pp* collisions, a new evaluation of the energy dependence of hadron production is performed within the NICA energy range. Results for mean multiplicities, rapidity spectra, and transverse momentum distributions of $\pi^{\pm}$, $K^{\pm}$, K^{0}_{S}, Λ, p, $\bar{p}$ are collected in the region of collision energies $3 < \sqrt{s_{NN}} < 31$ GeV. This new collection includes recent measurements from the CERN NA49 and NA61 experiments for multiple hadron species. The excitation function of the particle yields is analyzed against Redge- and Lund-model motivated fits and new parameterizations for hadron production cross-sections in inelastic proton-proton interactions are obtained. These results can be used for testing and tuning available microscopic models. In the study of the variation of the rapidity and transverse momentum spectra of hadrons with energy, an interesting scaling behavior of relevant parameters at NICA energies is observed. Based on this observation, a standalone algorithm for hadron phase space generation in *pp* collisions is suggested. This particle phase space generator was integrated into the MPD detector simulation framework and compared with the novel PHQMD generator.

7. FUNDING

This work was supported by the Russian Scientific Fund Grant 19-42-04101. Furthermore, we acknowledge support by the Deutsche Forschungsgemeinschaft (DFG, German Research Foundation).

REFERENCES

1. V. D. Kekelidze, R. Lednicky, V. A. Matveev, et al., "Three stages of the NICA accelerator complex," Eur. Phys. J. A **52**, 211 (2016).
2. V. Golovatyuk, V. Kekelidze, V. Kolesnikov, et al., "The multi-purpose detector (MPD) of the collider experiment," Eur. Phys. J. A **52**, 212 (2016).
3. C. Alt et al. (NA49 Collab.), "Pion and kaon production in central Pb + Pb collisions at 20A and 30A GeV: evidence for the onset of deconfinement," Phys. Rev. C **77**, 024903 (2008).
4. A. Palmese, W. Cassing, E. Seifert, et al., "Chiral symmetry restoration in heavy-ion collisions at intermediate energies," Phys. Rev. C **94**, 044912 (2016).
5. A. M. Rossi et al., "Experimental study of the energy dependence in proton proton inclusive reactions," Nucl. Phys. B **84**, 269 (1975).
6. M. Gazdzicki and D. Röhrich, "Strangeness in nuclear collisions," Z. Phys. C **71**, 55 (1996).
7. H. Weber et al., "Hadronic observables at relativistic energies: anything strange with strangeness?," Phys. Rev. C **67**, 014904 (2003).
8. M. Gazdzicki and D. Rohrich, "Pion multiplicity in nuclear collisions," Z. Phys. C **65**, 215 (1995).
9. C. Alt et al. (NA49 Collab.), "Inclusive production of charged pions in p + p collisions at 158 GeV/*c* beam momentum," Eur. Phys. J. C **45**, 343 (2006).
10. T. Anticic et al. (NA49 Collab.), "Inclusive production of charged kaons in p + p collisions at 158 GeV/c beam momentum and a new evaluation of the energy dependence of kaon production up to collider energies," Eur. Phys. J. C **68**, 1 (2010).
11. T. Anticic et al. (NA49 Collab.), "Inclusive production of protons, anti-protons and neutrons in p + p collisions at 158 GeV/c beam momentum," Eur. Phys. J. C **65**, 9 (2010).
12. N. Abgrall et al. (NA61/SHINE Collab.), "Measurement of negatively charged pion spectra in inelastic p + p interactions at p_lab= 20, 31, 40, 80 and 158 GeV/*c*," Eur. Phys. J. C **74**, 2794 (2014).
13. A. Aduszkiewicz et al. (NA61/SHINE Collab.), "Measurements of $\pi^{\pm}$, $K^{\pm}$, p and $\bar{p}$ spectra in proton-proton interactions at 20, 31, 40, 80 and 158 GeV/c with the NA61/SHINE spectrometer at the CERN SPS," Eur. Phys. J. C **77**, 671 (2017).
14. A. Aduszkiewicz et al. (NA61/SHINE Collab.), "Production of Λ-hyperons in inelastic p + p interactions at 158 GeV/*c*," Eur. Phys. J. C **76**, 198 (2016).
15. S. Afanasiev et al. (NA49 Collab.), "The NA49 large acceptance hadron detector," Nucl. Instrum. Methods Phys. Res., Sect. A **430**, 210 (1999).
16. N. Abgrall et al. (NA61/SHINE Collab.), "NA61/SHINE facility at the CERN SPS: beams and detector system," J. Instrum. **9**, 06005 (2014).
17. M. Antinucci et al., "Multiplicities of charged particles up to ISR energies," Lett. Nuovo. Cimento Soc. Ital. Fis. **6**, 121 (1973).
18. J. Adamczewski-Musch et al. (HADES Collab.), "Inclusive Λ production in proton-proton collisions at 3.5 GeV," Phys. Rev. C **95**, 015207 (2017).
19. D. M. Tow, "Average multiplicity, secondary trajectory, and Mueller analysis," Phys. Rev. D: Part. Fields **7**, 3535 (1973).
20. W. Cassing and E. L. Bratkovskaya, "Hadronic and electromagnetic probes of hot and dense nuclear matter," Phys. Rep. **308**, 65 (1999).
21. S. V. Afanasiev et al. (NA49 Collab.), "Production of ϕ-mesons in p + p, p + Pb and central Pb + Pb collisions at Ebeam = 158A GeV," Phys. Lett. B **491**, 59 (2000).
22. M. J. Menon and P. V. Silva, "A study on analytic parametrizations for proton–proton cross-sections and asymptotia," J. Phys. G **41**, 019501 (2014).
23. S. A. Bass et al., "Microscopic models for ultrarelativistic heavy ion collisions," Prog. Part. Nucl. Phys. **41**, 225 (1998).
24. T. Pierog and K. Werner, "EPOS model and ultra high energy cosmic rays," Nucl. Phys. Proc. Suppl. **196**, 102 (2009).
25. W. Ehehalt and W. Cassing, "Relativistic transport approach for nucleus nucleus collisions from SIS to SPS energies," Nucl. Phys. A **602**, 449 (1996).
26. J. Aichelin, E. Bratkovskaya, A. le F'evre, et al., arXiv: 1907.03860v1 [nucl-th] (2019).
27. http://mpd.jinr.ru.
28. J. Geiss, W. Cassing, and C. Greiner, "Strangeness production in the HSD transport approach from SIS to SPS energies," Nucl. Phys. A **644**, 107 (1998).
29. B. Anderson, G. Gustafson, and Hong Pi, "The FRITIOF model for very high energy hadronic collisions," Z. Phys. C **57**, 485 (1993).